

Near-Field Energy Transfer into Silicon Inversely Proportional to Distance Using Quasi-2D Colloidal Quantum Well Donors

Muhammad Hamza Humayun, Pedro Ludwig Hernandez-Martinez, Negar Gheshlaghi, Onur Erdem, Yemliha Altintas, Farzan Shabani, and Hilmi Volkan Demir*

Silicon is the most prevalent material system for light-harvesting applications; however, its inherent indirect bandgap and consequent weak absorption limits its potential in optoelectronics. This paper proposes to address this limitation by combining the sensitization of silicon with extraordinarily large absorption cross sections of quasi-2D colloidal quantum well nanoplatelets (NPLs) and to demonstrate excitation transfer from these NPLs to bulk silicon. Here, the distance dependency, d , of the resulting Förster resonant energy transfer from the NPL monolayer into a silicon substrate is systematically studied by tuning the thickness of a spacer layer (of Al_2O_3) in between them (varied from 1 to 50 nm in thickness). A slowly varying distance dependence of d^{-1} with 25% efficiency at a donor–acceptor distance of 20 nm is observed. These results are corroborated with full electromagnetic solutions, which show that the inverse distance relationship emanates from the delocalized electric field intensity across both the NPL layer and the silicon because of the excitation of strong in-plane dipoles in the NPL monolayer. These findings pave the way for using colloidal NPLs as strong light-harvesting donors in combination with crystalline silicon as an acceptor medium for application in photovoltaic devices and other optoelectronic platforms.

1. Introduction

Colloidal semiconductor nanocrystals (NCs), also known as artificial atoms, are on the vanguard as possible photonic materials on account of exhibiting unique optical and optoelectronic properties. Years of extensive research on these NCs have provided us with control over such properties of theirs by adjusting their shape, size, doping, alloying, and heterostructuring during the NC growth process.^[1] The combination of their physical properties and the ease of their solution-processable fabrication process open their scope as an attractive alternative to conventional semiconductors for a wide variety of photonic applications.^[2] Some of the properties of these nanostructures can also be further modified by using the electromagnetic interaction between these optical nano-emitters and the proximal inhomogeneity, such as a planar interface with a conventional semiconductor substrate.^[3,4]

Optical excitation in an emitter can lose its energy through radiative energy transfer (RET) and nonradiative energy transfer (NRET) processes.^[5] These energy transfer (ET) mechanisms are distance-dependent, and the strength of the ET process is largely determined by the separation of the donor emitter from an acceptor, for example, a substrate. RET is a longer-ranged mechanism in which the emitter emission couples into the photonic waveguide modes of a substrate.^[6] When the emitter is brought close to the substrate (typically less than 2 nm), excitons can be transferred nonradiatively via two-way charge transfer known as Dexter energy transfer (DET) or, for longer distances, through dipole-dipole coupling known as Förster resonance energy transfer (FRET).^[7] DET requires the wavefunction overlap, which can only happen if their separation is less than 2 nm. On the other hand, FRET stems from dipole-dipole interactions owing to the oscillating dipole field of the emitter, which nonradiatively excites the electron–hole pair in the acceptor and is effective over a distance of several nanometers.^[8]

Although several parameters, including photoluminescence (PL) quantum yield of the donor, absorption cross section of the acceptor, the orientation of the dipoles between the donor and acceptor, and the refractive index of the surrounding medium^[5,9–11] affect FRET, FRET is most sensitive to the distance between the donor and acceptor. The distance dependence

M. H. Humayun, P. L. Hernandez-Martinez, N. Gheshlaghi, O. Erdem, Y. Altintas, F. Shabani, H. V. Demir
Department of Electrical and Electronics Engineering
Department of Physics
UNAM – Institute of Materials Science and Nanotechnology
Bilkent University
Ankara 06800, Turkey
E-mail: volkan@bilkent.edu.tr

P. L. Hernandez-Martinez, H. V. Demir
LUMINOUS! Centre of Excellence for Semiconductor Lighting and Displays
The Photonics Institute
School of Electrical and Electronic Engineering
School of Physical and Mathematical Sciences
School of Materials Science and Engineering
Nanyang Technological University
Singapore 639798, Singapore
Y. Altintas
Department of Materials Science and Nanotechnology
Abdullah Gul University
Kayseri 38080, Turkey

 The ORCID identification number(s) for the author(s) of this article can be found under <https://doi.org/10.1002/sml.202103524>.

DOI: 10.1002/sml.202103524

of FRET itself, however, changes with the dimensionality of the donor and the acceptor. The FRET rate (Γ_{FRET}) between a donor–acceptor (D–A) pair typically follows the important power relationship, which dictates the effective range of ET

$$\Gamma_{\text{FRET}} \propto d^{-n} \quad (1)$$

where d is the separation between the donor and the acceptor and n is a positive real number. Here, n depends on different geometries of D–A pairs. Theoretically, it is expected to be 6 for 0D pairs, 4 for 0D–2D pairs, 2 for 2D–2D pairs, and 3 for 0D–3D (bulk) pairs.^[12,13] By fabricating hybrid structures with appropriate donor–acceptor pairs, we can therefore control their strengths to obtain highly efficient ET-based optoelectronic devices, including solar cells and light-emitting diodes (LEDs).

The quasi-0D NCs, commonly known as colloidal quantum dots (QDs), have been successfully used as energy donors with various exciton-sinking platforms from 3D bulk silicon^[14–16] to 2D transition metal dichalcogenides (TMDCs)^[17] and semimetals (e.g., graphene).^[18] In the last decade, quasi-2D NCs nicknamed nanoplatelets (NPLs) have emerged as promising solution-processed atomically-flat NCs.^[19,20] The salient feature of these quasi-2D quantum wells is the presence of strong anisotropy in their physical dimensions.^[21,22] These NPLs are a few monolayers thick with control over their vertical thickness possible in atomic precision.^[23–25] Their typical lateral dimensions are larger than the excitonic Bohr radius. Furthermore, the ultra-narrow vertical dimensions result in quasi-1D confinement of excitons in these NPLs. Consequently, NPLs possess very narrow emission linewidth (8–10 nm),^[26–28] giant oscillation strength,^[9,29,30] and large absorption cross sections.^[31] Such properties are highly desirable for a broad range of photonic studies and make them attractive for optoelectronic applications, including lasing,^[32–34] LEDs,^[35–38] and sensing.^[39–41]

A distinctly large absorption cross section makes NPLs uniquely promising and superior for light-harvesting applications wherein these NPLs can absorb photons and, subsequently, transfer their energy through the NRET to a substrate. NPLs are expected to outperform QDs as energy donors as NPLs possess a higher intrinsic absorption cross section compared to QDs.^[42] To date, studies involving NPLs have focused on the energy transfer in 2D–2D hybrid structures, where the NPLs function as the donor specie while the acceptor consists of NPLs^[43] or a 2D TMDC film.^[44] Or in a 0D–2D hybrid structure^[45] where QDs act as energy donors and NPLs act as the acceptor layer.

However, a study on the FRET in a 2D–3D hybrid structure, with silicon as the exciton-sinking medium, has not been explored at all to date. From an application point of view, silicon provides the most advanced, mature, and widely used semiconductor technology platform. However, silicon being an indirect bandgap material, suffers from relatively weak light absorption and reduces the efficiency of such silicon-based light-harvesting systems. Sensitization with a strong light absorber like NPLs can substantially enhance the poor absorption of silicon.^[8,16,46,47]

In the present study, we investigate FRET from a monolayer of CdSe/CdZnS core–shell NPLs into the silicon substrate. Here, thin alumina spacer layers with precise thickness control were deposited with varying thicknesses, using atomic layer deposition (ALD), to systematically study FRET-based distance dependence of the decay kinetics of the donor NPLs. The energy

transfer rate and efficiency were computed from measurements obtained using time-resolved fluorescence (TRF) spectroscopy. We found that the FRET efficiency scales with d^{-1} , where d is the distance between the donor NPL and the surface of the silicon substrate. These results were further confirmed using full electromagnetic modeling. The simulated trend of decay rates is in excellent agreement with the experimental results. In literature, the distance scaling for FRET from the point-like donor to the 3D acceptor is d^{-3} . The distance scaling for the FRET rate is expected to further drop when the donor has 2D geometry instead of being point-like.^[48] We show that the delocalized electric field owing to the self-assembled monolayer of NPLs and the strong in-plane dipole present in the anisotropic NPLs are the root cause of the d^{-1} distance dependency.

2. Experimental Section

The schematic representation of the hybrid structure used to study the ET from NPLs to the silicon wafer in this work is sketched in **Figure 1a**. Our model system consists of NPLs and silicon substrate separated by an alumina spacer. We define $d = d_L + t_{\text{NPL}/2} + t_{\text{Al}_2\text{O}_3} + t_{\text{SiO}_2}$ as the distance from the surface of the substrate to the NPL dipole, where $d_L = 2$ nm is the length of the ligands, $t_{\text{NPL}} = 4$ nm is the thickness of the core/shell NPLs (in which the exciton is assumed to be at the center of the core/shell), $t_{\text{SiO}_2} = 1.8$ nm is the thickness of the native oxide layer on top of the silicon surface, as confirmed by ellipsometry measurements, and $t_{\text{Al}_2\text{O}_3}$ is the thickness of the Al_2O_3 spacer. Al_2O_3 of varying thicknesses tuned from 1 to 50 nm was deposited via atomic layer deposition. These thicknesses were also confirmed using ellipsometry.

Figure 1b schematically depicts the E – k diagrams for the 1D quantum-confined NPLs and the indirect bandgap silicon illustrating the energy transfer processes, for which more discussion is further provided in Section 3. Here, NPLs were deposited onto the silicon-based substrates via a self-assembly method previously reported by our group (see the Supporting Information for the deposition details).^[49] This deposition technique ensures that all the NPLs are in face-down orientation and helps to avoid the formation of NPL multilayers, as shown in the scanning electron microscopy image in **Figure 1c**. The NPLs used in this study are made of CdSe/Cd_{0.25}Zn_{0.75}S core/shell heterostructure, synthesized using a hot injection method our group previously developed to coat robust shells (see the Supporting Information for the details of synthesis and optical characterization of the hetero-NPLs).^[50] These NPLs are cuboidal-shaped with a square-like lateral area with 17.2 ± 1.8 nm of edge and a vertical thickness of 4.4 ± 0.5 nm as deduced from the transmission electron microscopy (TEM) image shown in **Figure 1d**. **Figure 1e** presents the absorption and PL spectra of these NPLs, along with the optical absorption of silicon. Two absorption features centered at 633 and 575 nm in the NPL absorption are attributed to the electron–heavy hole and the electron–light hole transitions, respectively. The emission peak of the NPLs in the PL spectrum appears centered at 640 nm with a full-width-half-maximum (FWHM) of 23.9 nm.

For each sample with a particular spacer thickness, PL decay rates were collected through time-correlated single-photon counting (TCSPC) measurements at room temperature using

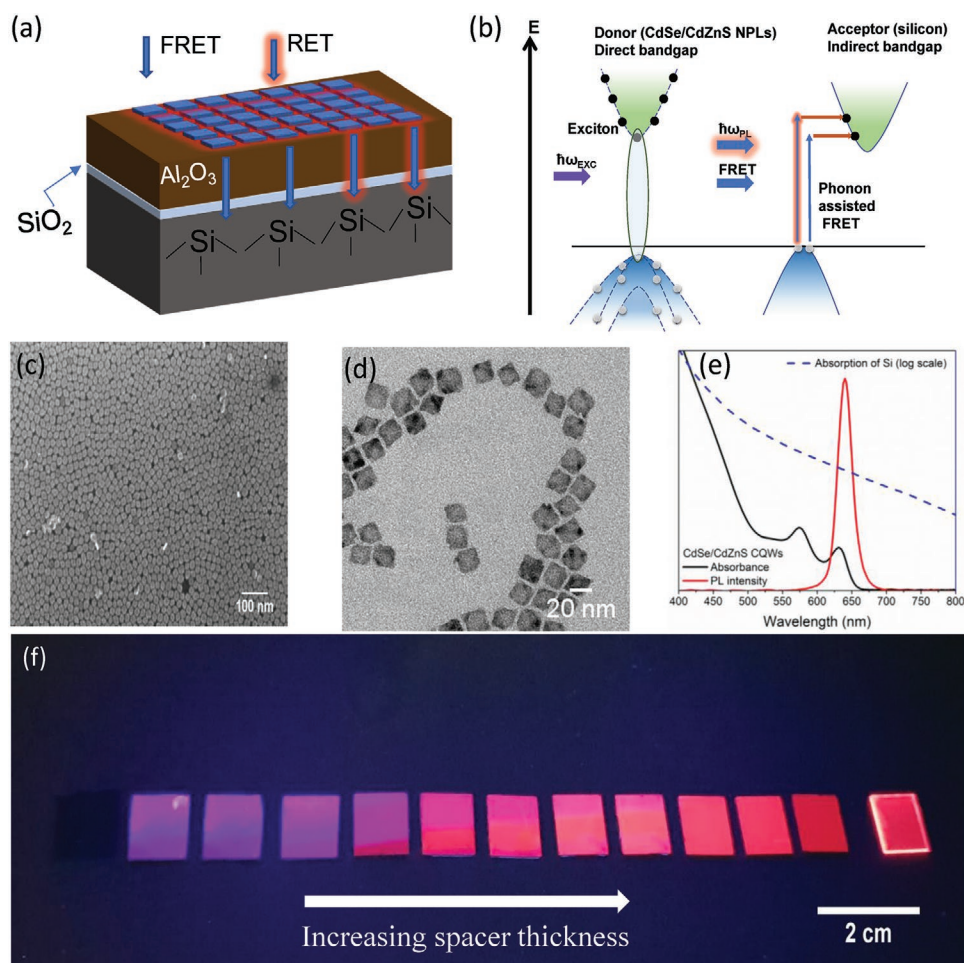


Figure 1. a) Schematic depiction of our hybrid NPL- Al_2O_3 -Si system. b) Energy band diagram illustrating the energy transfer from NPLs to crystalline silicon. c) Scanning electron microscopy image of self-assembled NPLs on the silicon substrate. d) Transmission electron microscopy image of the CdSe/CdZnS core/shell NPLs. e) Normalized photoluminescence and UV–vis absorption spectra of the CdSe/CdZnS core/hot-injection shell NPLs (donor) and absorption spectrum of silicon. f) Photography of the samples illuminated by a 365 nm UV lamp: Samples are placed with increasing Al_2O_3 spacer thicknesses.

a time-resolved fluorescence spectrometer (FluoTime 200, Pico-Quant), which was equipped with a pulsed pump laser as an excitation source (wavelength of 375 nm, pulse width ≈ 200 ps, pulse repetition rate 2.5 MHz). Fluorescence lifetimes were recorded at the peak emission wavelength of the NPLs. The decays were fit to biexponential curves convolved with the instrument response function (see Table S1, Supporting Information, for the complete fitting parameters). Optical characterization was carried out using UV–visible absorbance and PL spectroscopy.

3. Results

The energy transfer process between the donor NPLs and the indirect Si acceptor is illustrated in Figure 1b. When the NPLs are illuminated by an excitation source, electron–hole pairs are photogenerated. In the NPLs, the excited electrons relax to the lowest level of the excited state in a matter of picoseconds or less, a phenomenon known as internal conversion. These

photogenerated excitons can then decay through FRET and RET channels and return to the ground state, as sketched in the figure. Since silicon is an indirect bandgap semiconductor, transitions from ground to the excited state in silicon require a phonon to compensate for the momentum mismatch (details of this phonon-assisted process are discussed in our previous work^[14]).

Figure 1f presents the photographs of fluorescence quenching when the samples with carefully tuned Al_2O_3 spacers are irradiated by a UV lamp. Here, it is observed that when NPLs are closer to the substrate, the emitted light is quenched as compared to when the emitters are further away from the substrate. To elaborate on this fluorescence quenching quantitatively, TRF measurements were performed on this set of samples with systematically varied spacer thicknesses as well as on an NPL film deposited on quartz, which is used as the only-donor sample. The obtained decays, plotted in Figure 2a, show the progressive reduction in donor lifetime as the spacer becomes thinner, which results from the increasing strength of FRET from the NPL to the silicon

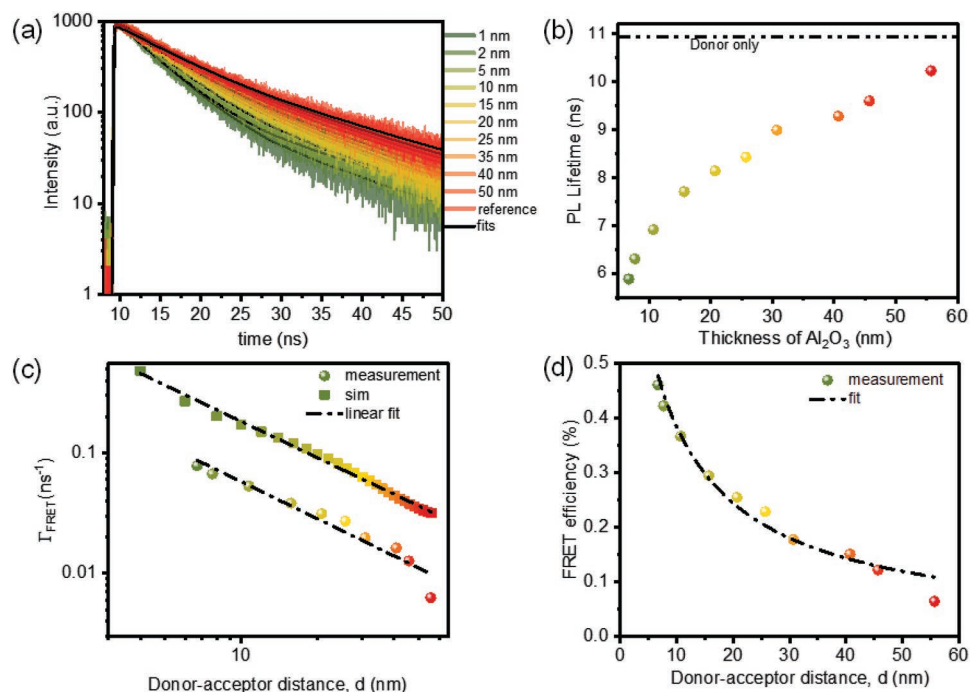


Figure 2. a) PL decay curves of the solid films collected at the donor PL emission peak with varying thickness of the Al₂O₃ separation layer. The solid black lines represent the fits of the curves. b) Amplitude-averaged lifetimes of the solid samples as a function of the spacer thickness. The dashed line indicates the only-donor lifetime. c) FRET rate, obtained from measured lifetimes and through electromagnetic solutions, as a function of the center-to-surface distance between the donor and the acceptor plotted on a logarithmic scale. The black dashed line is the linear fitting. d) FRET efficiency as a function of the center-to-surface distance between the donor and the acceptor. The black dashed line is the fitting made using Equation (4).

substrate.^[51] The NPLs-on-quartz structure models the scenario where NPLs are deposited on a semi-infinite dielectric layer. Decay kinetics of the donor NPLs indicate progressive acceleration as the thickness of the spacer layer is decreased, exhibiting a reduction in the lifetime as emitters come nearer to the substrate, demonstrating the distance-dependent energy transfer that is taking place.

The amplitude-averaged lifetimes are plotted in Figure 2b. Lifetimes are extracted by using bi-exponential decay fitting curves, $I(t) = A_1e^{-t/\tau_1} + A_2e^{-t/\tau_2}$, and then averaged over the amplitudes of the components, i.e., $\tau_{avg} = (A_1\tau_1 + A_2\tau_2) / (A_1 + A_2)$ (Supporting Information). Biexponential fitting revealed that the donor-only sample has an average lifetime of $\tau_D = 10.93$ ns, whereas the average lifetime reduces to 5.86 ns for the NPLs deposited with a 1 nm spacer layer present. From Figure 2b, it can be observed that the magnitude of the average lifetime increases (and the decay rate slows down) as the spacer thickness is increased. This shortening of the decay lifetimes with the reduced spacer thickness suggests that the coupling of the NPL dipole field with the silicon growing progressively stronger. This coupling results in the creation of an additional nonradiative channel via resonant energy transfer. The new channel could also be attributed to charge transfer between NPLs donor and bulk acceptor. However, the charge transfer requires extreme proximity between donor and acceptor species, generally less than 1 nm,^[7] which is not possible in our hybrid configuration because of the presence of a native oxide layer (2 nm) on the substrate as well as passivating ligands (2 nm) surrounding the NPLs.

The experimental FRET rates, Γ_{FRET} , can then be found using the measured lifetimes as

$$\Gamma_{FRET} = \frac{1}{\tau_{FRET}} = \frac{1}{\tau_{DA}} - \frac{1}{\tau_D} \quad (2)$$

where τ_D is the lifetime of the donor-only sample (reference sample) and τ_{DA} is the donor lifetime in the presence of the acceptor. Figure 2c shows Γ_{FRET} calculated from Equation (2) plotted as a function of the donor-acceptor distance d (represented by circular markers in the figure). The plot is on a logarithmic scale, and the linear fitting of this plot reveals the slope to be -1.02 . Therefore, in contrast to the strong distance dependence between the donor-acceptor pair with dimensionalities as explained in the Introduction, here we observe that the strength of FRET is considerably less sensitive to the distance and is virtually inversely proportional to the donor-acceptor distance.

Figure 2d shows η_{FRET} of the samples, which is calculated using Equation (3), as a function of the donor-acceptor distance d

$$\eta_{FRET} = 1 - \frac{\tau_{DA}}{\tau_D} \quad (3)$$

FRET efficiency's distance dependency was further examined using the following expression

$$\eta_{FRET} = \frac{1}{(1 + (d/d_0)^n)} \quad (4)$$

where d_0 is the Förster radius, and n is the exponent indicating the dependence of the FRET rate on the distance. By numerically fitting Equation (4) to the data obtained from Equation (3), we found d_0 to be 6.1 nm and $n = 0.95$. Therefore, after analyzing the experimental results for our hybrid structure, we conclude that the FRET is taking place in our system, and the energy transfer rate scales with the inverse of the NPL dipole–silicon separation.

4. Theory and Discussion

To further understand these experimental results, the full numerical electromagnetic solution was performed to compute the FRET rates as well as to obtain the electric field maps in the NPL and the acceptor region. NPL excitons are modeled by placing point electric dipoles within an NPL layer at a distance d from the substrate. The FRET rate to the dielectric layer with in-plane and perpendicular dipole orientations is found using^[44,52–55]

$$\Gamma_{FRET} = \frac{2Im(\epsilon_{si}(\omega))}{4\pi\hbar} \int \mathbf{E} \cdot \mathbf{E}^* dV \quad (5)$$

where $\epsilon_{si}(\omega) = 16 + j0.3$ is the complex dielectric constant of silicon at the peak emission wavelength of the donor NPL,^[56] and \mathbf{E} is the induced electric field distribution in the volume of the silicon substrate. The dielectric constant of NPLs used in the simulations was taken to be that of bulk CdSe at the peak emission wavelength of the NPL. We placed oscillating dipoles within the NPL layer and calculated the induced electric field inside the silicon region numerically. The simulations were performed with four dipoles present inside the NPL layer. They form vertices of a unit square whose side lengths equal the center-to-center distance between the two neighboring NPLs with only ligand spacing present, which is the scenario in our self-assembled NPL layers. For comparison, we also simulated a single dipole present in the NPL layer. By simulating the electric field distribution, we evaluated the FRET rate using Equation (5), from which it can be seen that the decay rate is proportional to the imaginary component of the dielectric function of the acceptor medium and the integrated intensity in the acceptor layer due to the radiating dipole. All simulations were

carried out for both in-plane and out-of-plane dipole orientation. The average FRET rate is^[57]

$$\Gamma_{FRET} = \frac{(2 \times \Gamma_{\parallel} + \Gamma_{\perp})}{3} \quad (6)$$

where Γ_{\perp} and Γ_{\parallel} are the rate of FRET due to the out-of-plane and in-plane dipoles, respectively.

The FRET rate was then numerically obtained for varying spacer thicknesses. The donor–acceptor separation in our case is well shorter than the wavelength of the photon emitted by a dipole so that we can safely rule out the far-field ET mechanism. Therefore, in our setup, we do not expect the generation of electron–hole pairs in the silicon layer due to photons emitted by the excited NPLs. Instead, energy migration is dominated by the dipole–dipole interaction between the donor–acceptor pair.

Figure 2c shows the comparison between FRET rates obtained from measurements and the simulation as a function of the donor–acceptor distance (simulation data points represented by square markers in the figure). The slope obtained from linear fitting the simulated FRET rate data is -1.01 , thus, following the same trend as the experimental results, suggesting successful modeling of our experimental setup. There is an overshoot in the magnitude because numerical simulation results are obtained through ideal modeling. The offset could be a result of the simplifications adopted to facilitate simulations. In setting up our numerical model, we have not taken into account the thin native oxide layer. Also, we have not taken into consideration the ligands attached to the NPLs. Another assumption used in our model is that nanocrystals form a perfect 2D layer. In doing so, we have ignored the presence of voids and edge effects from individual NPLs.

To further expound on the d^{-1} dependency of the energy transfer, we investigated the electric field distribution inside NPL and silicon regions for different orientations of the dipoles as well as for different spacer thicknesses. We observed that the electric field intensity inside silicon is more delocalized, drops more gradually, and penetrates further for the in-plane dipole orientation than the out-of-plane component. We, therefore, conclude that it is the in-plane dipole orientation that dictates the d^{-1} dependence. **Figure 3** exhibits the electric field intensity

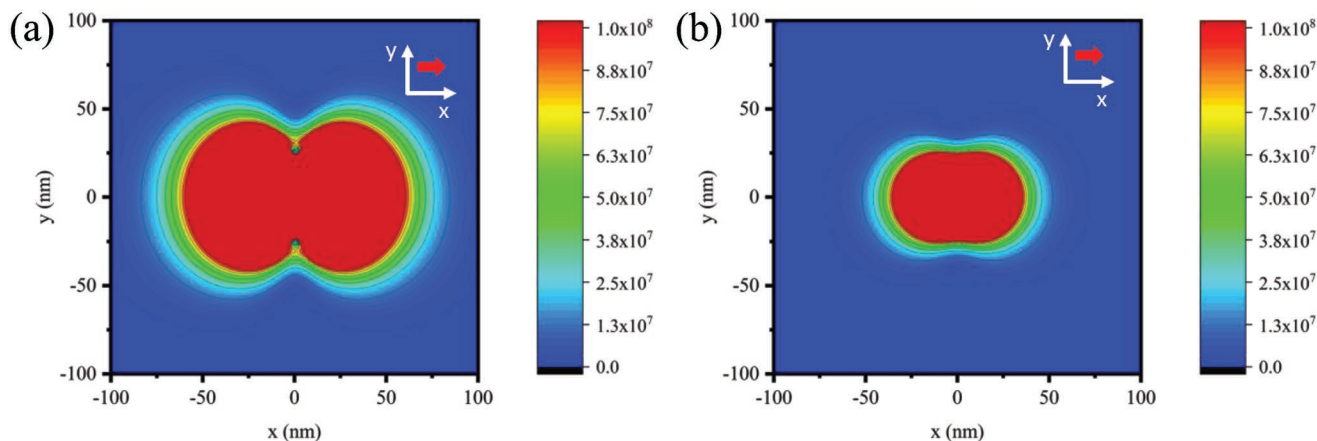


Figure 3. Electric-field Intensity at the NPL layer: a) four uniformly distributed dipoles present oriented in-plane and b) single dipole oriented in-plane.

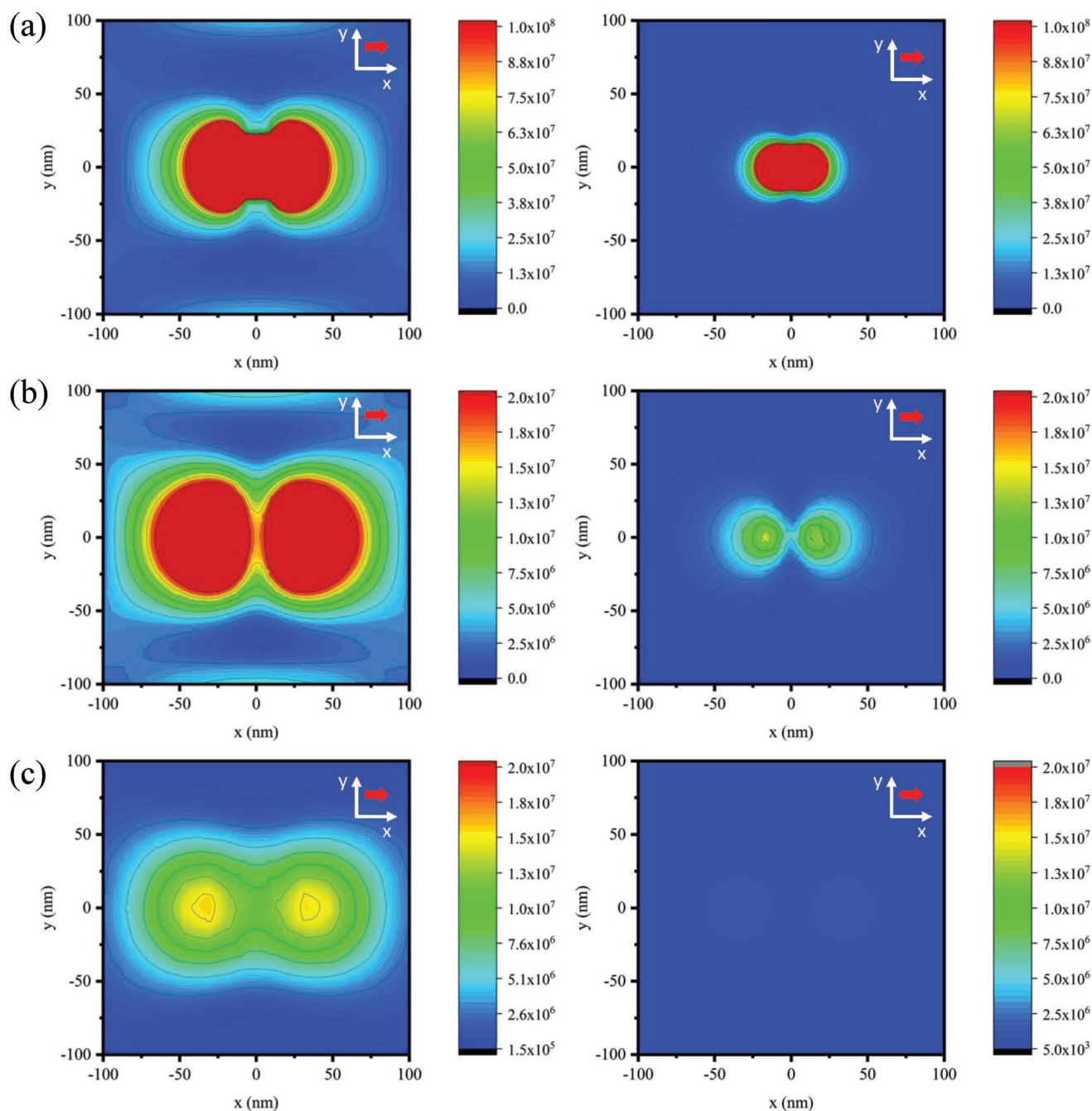


Figure 4. Comparison between $|E|^2$ field distribution on the XY-plane within silicon region 2 nm below the surface for four uniformly distributed dipoles present, oriented in-plane (left column) with that of single dipole oriented in-plane (right column) with Al₂O₃ spacer thickness of a) 2 nm, b) 20 nm, and c) 50 nm.

inside the NPL layer where the dipoles reside. We observe the enhancement in the electric field delocalization with the multiple dipoles present. **Figure 4** shows the electric field distribution inside the silicon domain at a level 2 nm below the surface for Al₂O₃ thicknesses of 2, 20, and 50 nm. Compared to the single NPL case, we see that the electric field is further extended across the silicon layer in the presence of multiple dipoles. The drop in the electric field intensity for multiple in-plane oriented model is lesser than the rest of the models.

Figure 5 displays the electric field maps along the xz cross section within the silicon layer for Al₂O₃ thicknesses: 2, 20, and 50 nm. We observe that when multiple dipoles are oriented in-plane, the electric field penetrates deeper into the silicon layer, and at the same time, is a lot stronger and delocalized compared to other models. In our previous work,^[44] it has been shown that the FRET rate's distance dependence to be d^{-2} for a hybrid structure consisting of NPLs and 2D MoS₂ monolayer. Herein, we have extended the geometry in the third

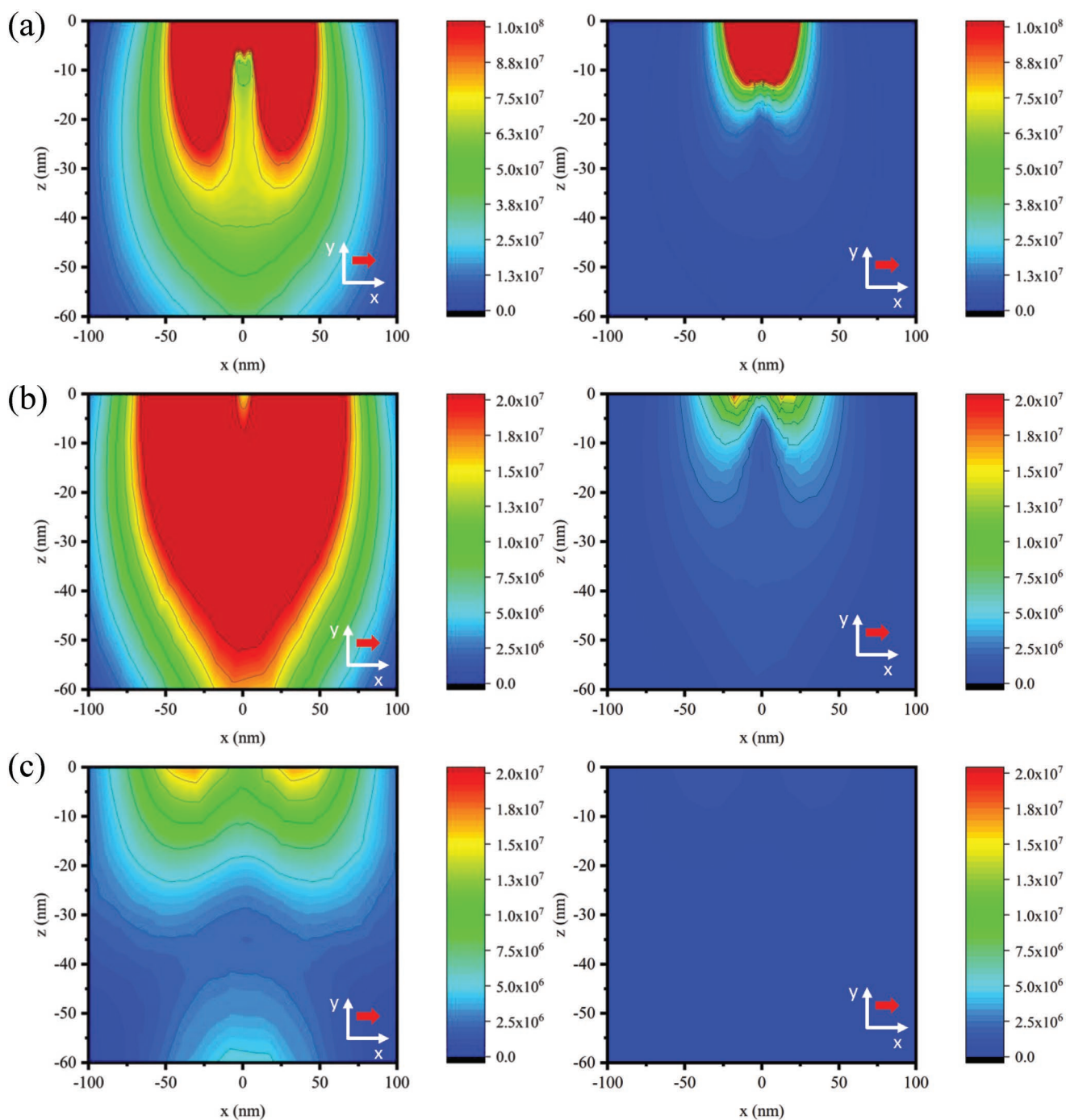


Figure 5. Electric field intensity distribution on the XZ-plane ($y=0$) within silicon region for four uniformly distributed dipoles present, oriented in-plane (left column) with that of single dipole oriented in-plane (right column) with Al_2O_3 spacer thickness of a) 2 nm, b) 20 nm, and c) 50 nm.

dimension by using a bulk acceptor and observe that the FRET rate distance sensitivity decreases further. Therefore, for this self-assembled 2D NPL layer, the dominant dipole components are oriented along lateral dimensions of the NPL. These results suggest that the electric field delocalization due to the coupling in the NPL layer and electric field distribution in the bulk silicon layer induced by the in-plane oriented dipoles present in the NPL layer results in the energy transfer rate scaling with $1/d$.

To finalize our study, we show a proof-of-concept demonstration where we measured the photocurrent enhancement factor for a set of Si-based photodetectors with Al Schottky contacts, as shown in **Figure 6a** (see the Supporting Information for details of the device fabrication and characterization). The photodetectors are deposited with Al_2O_3 spacer layer of carefully tuned thickness. Figure 6b presents the photocurrent enhancement factor parameterized with respect to the spacer

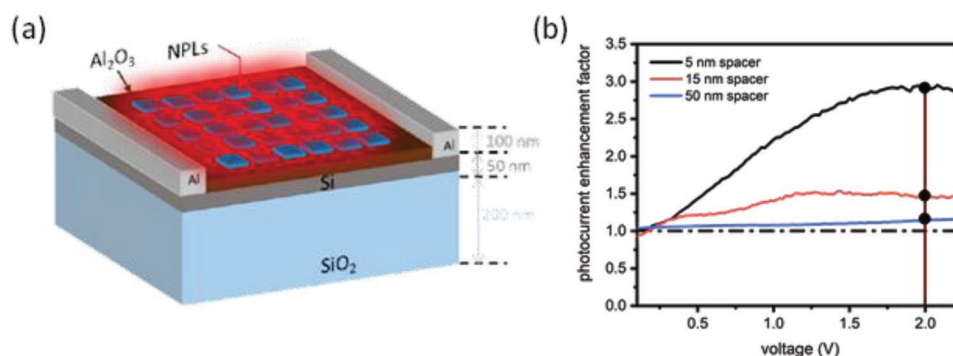


Figure 6. a) Schematic of our proof-of-concept device. b) Photocurrent enhancement owing to the presence of NPLs atop an ultrathin Si photodetector with respect to the negative control group device with no NPLs. Photocurrent enhancement factor as a result of the NPL deposition for the spacer thicknesses of 5, 15, and 50 nm.

thicknesses of 5, 15, and 50 nm. The photocurrent enhancement factor is calculated by taking the ratio of the illumination current to dark current before and after NPL deposition (the absolute photocurrent measurement obtained by subtracting the dark current from the current of the device under illumination is shown in Figure S4, Supporting Information). We observe an overall improvement in the photocurrent for all spacer thickness with the best performance for the 5 nm case. This case has a maximum boost of ≈ 3 times (300%) at 2 V bias. These results demonstrate that the silicon photocurrent can be enhanced using NPLs proximal to the silicon layer. Improving the optical response of silicon can greatly benefit photovoltaic and other optoelectronic applications.

5. Conclusions

In summary, we have experimentally studied the effect of the indirect bandgap silicon substrate on the emission kinetics of the colloidal quasi-2D quantum wells in close proximity. We systematically adjusted the separation between the self-assembled NPL monolayer and the substrate surface by depositing a spacer layer of Al₂O₃ at carefully tuned thicknesses and observed the resulting modification in the lifetime of the NPL ensemble. We found the FRET to be the dominant cause for the change of the PL decays. Our experimental results revealed that photosensitization of silicon with a monolayer of quasi-2D nano-emitters results in energy transfer rates inversely proportional to the distance between the NPLs and the silicon substrate. These experimental results have been further corroborated using a full numerical electromagnetic solution, which demonstrates that the d^{-1} dependence is due to electric field delocalization due to strong in-plane dipoles in the NPLs. These findings indicate that such face-down oriented NPL assembly is highly favorable for strong NRET-based photosensitization on Si towards enhanced light-harvesting.

Supporting Information

Supporting Information is available from the Wiley Online Library or from the author.

Acknowledgements

The authors gratefully acknowledge the financial support in part from Singapore National Research Foundation under the programs of NRFNRF12016-08 and the Science and the Singapore Agency for Science, Technology and Research (A*STAR) SERC Pharos Program under Grant No.152-73-00025 and in part from TUBITAK 115F297, 117E713, and 119N343. H.V.D. also acknowledges support from TUBA. O.E. acknowledges TUBITAK for financial support through the BIDEB-2211 program. The authors also thank Mr. Huseyin Bilge Yagci for his assistance in taking the photocurrent measurements.

Conflict of Interest

The authors declare no conflict of interest.

Data Availability Statement

The data that support the findings of this study are available from the corresponding author upon reasonable request.

Keywords

colloidal nanoplatelets, distance dependency, FRET, nonradiative energy transfer, self-assembly, semiconductor nanocrystals, silicon

Received: June 16, 2021

Revised: July 18, 2021

Published online: September 12, 2021

- [1] M. V. Kovalenko, L. Manna, A. Cabot, Z. Hens, D. V. Talapin, C. R. Kagan, V. I. Klimov, A. L. Rogach, P. Reiss, D. J. Milliron, P. Guyot-Sionnest, G. Konstantatos, W. J. Parak, T. Hyeon, B. A. Korgel, C. B. Murray, W. Heiss, *ACS Nano* **2015**, *9*, 1012.
- [2] Y. Yin, A. P. Alivisatos, *Nature* **2005**, *437*, 664.
- [3] L. Novotny, B. Hecht, *Principles of Nano-Optics*, Cambridge University Press, Cambridge **2006**.
- [4] M. Pelton, *Nat. Photonics* **2015**, *9*, 427.
- [5] P. L. Hernández-Martínez, A. O. Govorov, H. V. Demir, *J. Phys. Chem. C* **2013**, *117*, 10203.
- [6] W. Peng, S. M. Rupich, N. Shafiq, Y. N. Gartstein, A. V. Malko, Y. J. Chabal, *Chem. Rev.* **2015**, *115*, 12764.

- [7] B. Guzelurk, H. V. Demir, *Adv. Funct. Mater.* **2016**, *26*, 8158.
- [8] L. Danos, N. R. Halcovitch, B. Wood, H. Banks, M. P. Coogan, N. Alderman, L. Fang, B. Dzurinak, T. Markvart, *Faraday Discuss.* **2020**, *222*, 405.
- [9] M. Olutas, B. Guzelurk, Y. Kelestemur, K. Gungor, H. V. Demir, *Adv. Funct. Mater.* **2016**, *26*, 2891.
- [10] R. M. Clegg, *Curr. Opin. Biotechnol.* **1995**, *6*, 103.
- [11] J. R. Lakowicz, *Principles of Fluorescence Spectroscopy*, Springer, New York **2006**.
- [12] A. L. Rogach, *Nano Today* **2011**, *6*, 355.
- [13] X. Liu, J. Qiu, *Chem. Soc. Rev.* **2015**, *44*, 8714.
- [14] A. Yeltik, B. Guzelurk, P. L. Hernandez-Martinez, A. O. Govorov, H. V. Demir, *ACS Nano* **2013**, *7*, 10492.
- [15] M. T. Nimmo, L. M. Caillard, W. De Benedetti, H. M. Nguyen, O. Seitz, Y. N. Gartstein, Y. J. Chabal, A. V. Malko, *ACS Nano* **2013**, *7*, 3236.
- [16] H. M. Nguyen, O. Seitz, W. Peng, Y. N. Gartstein, Y. J. Chabal, A. V. Malko, *ACS Nano* **2012**, *6*, 5574.
- [17] A. Raja, A. Montoya-Castillo, J. Zultak, X. X. Zhang, Z. Ye, C. Roquelet, D. A. Chenet, A. M. van der Zande, P. Huang, S. Jockusch, J. Hone, D. R. Reichman, L. E. Brus, T. F. Heinz, *Nano Lett.* **2016**, *16*, 2328.
- [18] L. Gaudreau, K. J. Tielrooij, G. E. D. K. Prawiroatmodjo, J. Osmond, F. J. García De Abajo, F. H. L. Koppens, *Nano Lett.* **2013**, *13*, 2030.
- [19] S. Ithurria, B. Dubertret, *J. Am. Chem. Soc.* **2008**, *130*, 16504.
- [20] S. Ithurria, G. Bousquet, B. Dubertret, *J. Am. Chem. Soc.* **2011**, *133*, 3070.
- [21] H. Halim, J. Simon, I. Lieberwirth, V. Mailänder, K. Koynov, A. Riedinger, *J. Mater. Chem. B* **2020**, *8*, 146.
- [22] A. W. Achtstein, A. Antanovich, A. Prudnikau, R. Scott, U. Woggon, M. Artemyev, *J. Phys. Chem. C* **2015**, *119*, 20156.
- [23] E. Lhuillier, S. Ithurria, A. Descamps-mandine, T. Douillard, R. Castaing, X. Z. Xu, P. Taberna, P. Simon, H. Aubin, B. Dubertret, *J. Phys. Chem. C* **2015**, *119*, 21795.
- [24] M. Dufour, J. Qu, C. Greboval, C. Méthivier, E. Lhuillier, S. Ithurria, *ACS Nano* **2019**, *13*, 5326.
- [25] E. Lhuillier, S. Pedetti, S. Ithurria, B. Nadal, H. Heuclin, B. Dubertret, *Acc. Chem. Res.* **2015**, *48*, 22.
- [26] Y. Kelestemur, B. Guzelurk, O. Erdem, M. Olutas, T. Erdem, C. F. Usanmaz, K. Gungor, H. V. Demir, *J. Phys. Chem. C* **2017**, *121*, 4650.
- [27] M. D. Tessier, B. Mahler, B. Nadal, H. Heuclin, S. Pedetti, B. Dubertret, *Nano Lett.* **2013**, *13*, 3321.
- [28] J. F. Specht, R. Scott, M. C. Castro, S. Christodoulou, G. H. V. Bertrand, A. V. Prudnikau, A. Antanovich, L. D. A. Siebbeles, N. Owschimikow, I. Moreels, M. Artemyev, U. Woggon, A. W. Achtstein, M. Richter, *Nanoscale* **2019**, *11*, 12230.
- [29] S. Ithurria, M. D. Tessier, B. Mahler, R. P. S. M. Lobo, B. Dubertret, A. L. Efos, *Nat. Mater.* **2011**, *10*, 936.
- [30] A. W. Achtstein, A. Schliwa, A. Prudnikau, M. Hardzei, M. V. Artemyev, C. Thomsen, U. Woggon, *Nano Lett.* **2012**, *12*, 3151.
- [31] A. Yeltik, S. Delikanli, M. Olutas, Y. Kelestemur, B. Guzelurk, H. V. Demir, *J. Phys. Chem. C* **2015**, *119*, 26768.
- [32] A. A. Rossinelli, H. Rojo, A. S. Mule, M. Aellen, A. Cocina, E. De Leo, R. Schäublin, D. J. Norris, *Chem. Mater.* **2019**, *31*, 9567.
- [33] N. Taghipour, S. Delikanli, S. Shendre, M. Sak, M. Li, F. Isik, I. Tanriover, B. Guzelurk, T. C. Sum, H. V. Demir, *Nat. Commun.* **2020**, *11*, 3305.
- [34] B. Guzelurk, M. Pelton, M. Olutas, H. V. Demir, *Nano Lett.* **2019**, *19*, 277.
- [35] Y. Kelestemur, Y. Shynkarenko, M. Anni, S. Yakunin, M. L. De Giorgi, M. V. Kovalenko, *ACS Nano* **2019**, *13*, 13899.
- [36] Z. Wen, C. Zhang, Z. Zhou, B. Xu, K. Wang, K. L. Teo, X. W. Sun, *IEEE J. Quantum Electron.* **2020**, *56*, 3200106.
- [37] B. Liu, Y. Altintas, L. Wang, S. Shendre, M. Sharma, H. Sun, E. Mutlugun, H. V. Demir, *Adv. Mater.* **2020**, *32*, 202070054.
- [38] Y. Altintas, B. Liu, P. L. Hernández-Martínez, N. Gheshlaghi, F. Shabani, M. Sharma, L. Wang, H. Sun, E. Mutlugun, H. V. Demir, *Chem. Mater.* **2020**, *32*, 7874.
- [39] X. Fan, D. Knepe, V. Sayevich, H. Kleemann, A. Tahn, K. Leo, V. Lesnyak, A. Eychmüller, *J. Phys. Chem. Lett.* **2019**, *10*, 4025.
- [40] A. Medda, A. Dutta, D. Bain, M. K. Mohanta, A. De Sarkar, A. Patra, *J. Phys. Chem. C* **2020**, *124*, 19793.
- [41] E. Lhuillier, A. Robin, S. Ithurria, H. Aubin, B. Dubertret, *Nano Lett.* **2014**, *14*, 2715.
- [42] L. Kubie, B. A. Parkinson, *Langmuir* **2019**, *35*, 5997.
- [43] A. Yeltik, M. Olutas, M. Sharma, K. Gungor, H. V. Demir, *J. Phys. Chem. C* **2019**, *123*, 1470.
- [44] N. Taghipour, P. L. Hernandez-Martinez, A. Ozden, M. Olutas, D. Dede, K. Gungor, O. Erdem, N. K. Perkgoz, H. V. Demir, *ACS Nano* **2018**, *12*, 8547.
- [45] O. Erdem, K. Gungor, B. Guzelurk, I. Tanriover, M. Sak, M. Olutas, D. Dede, Y. Kelestemur, H. V. Demir, *Nano Lett.* **2019**, *19*, 4297.
- [46] N. Alderman, L. Danos, L. Fang, M. C. Gressel, T. Markvart, *Chem. Commun.* **2017**, *53*, 12120.
- [47] L. Fang, K. S. Kiang, N. P. Alderman, L. Danos, T. Markvart, *Opt. Express* **2015**, *23*, A1528.
- [48] R. S. Swathi, K. L. Sebastian, *J. Chem. Sci.* **2009**, *121*, 777.
- [49] O. Erdem, S. Foroutan, N. Gheshlaghi, B. Guzelurk, Y. Altintas, H. V. Demir, *Nano Lett.* **2020**, *20*, 6459.
- [50] Y. Altintas, K. Gungor, Y. Gao, M. Sak, U. Quliyeva, G. Bappi, E. Mutlugun, E. H. Sargent, H. V. Demir, *ACS Nano* **2019**, *13*, 10662.
- [51] F. Prins, A. Sumitro, M. C. Weidman, W. A. Tisdale, *ACS Appl. Mater. Interfaces* **2014**, *6*, 3111.
- [52] P. L. Hernández-Martínez, A. O. Govorov, *Phys. Rev. B* **2008**, *78*, 035314.
- [53] V. M. Agranovich, G. C. La Rocca, F. Bassani, *JETP Lett.* **1997**, *66*, 748.
- [54] V. M. Agranovich, Y. N. Gartstein, M. Litinskaya, *Chem. Rev.* **2011**, *111*, 5179.
- [55] A. O. Govorov, J. Lee, N. A. Kotov, *Phys. Rev. B* **2007**, *76*, 125308.
- [56] D. E. Aspnes, A. A. Studna, *Phys. Rev. B* **1983**, *27*, 985.
- [57] P. L. Hernández-Martínez, A. O. Govorov, H. V. Demir, *J. Phys. Chem. C* **2014**, *118*, 4951.